



Science Arts & Métiers (SAM)

is an open access repository that collects the work of Arts et Métiers Institute of Technology researchers and makes it freely available over the web where possible.

This is an author-deposited version published in: <https://sam.ensam.eu>
Handle ID: <http://hdl.handle.net/10985/22295>



This document is available under CC BY-NC-ND license

To cite this version :

Gaël Le COZ, Laurent PELTIER, Romain PIQUARD, Pascal LAHEURTE, D'acunto ALAIN -
Machinability of TiNb bio-compatible alloys - Procedia CIRP - Vol. 110, p.59-63 - 2022

Any correspondence concerning this service should be sent to the repository

Administrator : scienceouverte@ensam.eu



V CIRP Conference on Biomanufacturing

Machinability of TiNb bio-compatible alloys

Gaël Le Coz^{a*}, Laurent Peltier^a, Romain Piquard^a, Pascal Laheurte^a, Alain D'Acunto^a^aLEM3 UMR CNRS

7 rue Félix Savart 57070 METZ France

* Corresponding author. Tel.: +33 3 55 00 41 52; E-mail address: gael.lecoz@univ-lorraine.fr**Abstract**

The success of biomedical implantation is linked to osseointegration, depending on the mechanical loading of the bone interface. The large difference in stiffness between the host bone (30 GPa) and the usual implant material (over 100 GPa), as well as the absence of mechanical stress at the surrounding bone, induce a stress shielding effect, which leads to bone atrophy and implant loss. A recent work has shown the possibility to produce so-called second-generation titanium alloys. β -type Ti alloys have been studied for biomedical applications, due to the composition of non-cytotoxic elements. Some TiNb alloys can reach after heat treatment a Young's modulus close to 35 GPa, which is really close to bone's one. Unfortunately, titanium and its alloys are well known for their poor machinability due to the hardness and low thermal conductivity. Machined surfaces of titanium alloys are also easily damaged (micro cracks, build-up edge, plastic deformation, heat-affected zones, and tension residual stresses) during the process. Studying process parameters is important to avoid these phenomena.

The machinability of TiNb (turning, milling) has not been studied to date. Therefore, in this study, we examined the behavior of the TiNb titanium alloy for applications as a biomaterial in micro-cutting. Orthogonal cutting tests were performed on austenite and martensite states TiNb alloys and compared with Ti40 pure titanium. The aim was to evaluate the influence of the alloys and the cutting parameters on the evolution of the cutting forces, specific cutting energy, friction coefficient which are good indicators of machinability

© 2022 The Authors. Published by Elsevier B.V.

This is an open access article under the CC BY-NC-ND license (<https://creativecommons.org/licenses/by-nc-nd/4.0>)

Peer-review under responsibility of the scientific committee of the V CIRP Conference on Biomanufacturing

Keywords: Type your keywords here, separated by semicolons ;**1. Introduction**

The formation of the interface between living bone and biomedical implants, as known as osseointegration, depends on mechanical loading at this interface. For example, a large gap of stiffnesses between material implant and bone (30 GPa) or no mechanical stress at the surrounding bone leads to stress shielding effects. Bone atrophy and implant loss can occur [1,2], and additional surgery is necessary [3-6].

Ti-6Al-4V is widely used for biomedical implants and has interesting properties such as a low density, a high resistance to fatigue and corrosion. However, its stiffness is relatively high

(110GPa). Vanadium ions are cytotoxic and can reduce osseointegration and aluminum ions can cause neurological disorders and Alzheimer's disease [7-9].

Recent work has shown the possibility to produce titanium alloys composed of non-cytotoxic elements. These β -type Ti alloys have been studied for biomedical applications. These alloys are β -metastable, and a martensitic transformation can occur under stress by the formation of an α phase [10] This phase transformation, possible due to the instability of the β -phase, depending on the chemical compositions, enables interesting effects such as superelasticity effect (SE) or shape memory effect (SME). This phase transformation in the binary

* Corresponding author. Tel.: +33-355-004-152.

E-mail address: gael.lecoz@univ-lorraine.fr

alloy Ti-24Nb has been studied by Elmay et al [11]. This alloy reached a Young's modulus close to 35 GPa after heat treatment. The low modulus is generating a growing interest from the medical implant industry but to consider an industrialization of the process, an understanding of the material cut must be considered.

To achieve the requirements of medical such as surface quality or miniaturization, precise machining is needed [12]. With a low thermal conductivity and high hardness, Titanium alloys have a poor machinability. Damages (micro-cracks, heat-affected zones or residual stresses) are often observed on machined surfaces [13]. Concerning the machining of shape memory and superelastic alloys, studies have been carried out on NiTi in the medical field [14-16]. The high ductility, the unconventional strain-stress behavior and the high degree of work hardening of NiTi alloys during cutting leads to difficult processing, poor workpiece quality, burr formation and tool wear.

Concerning the machinability of TiNb, literature is poor. This study investigates its machining for biomedical applications. TiNb alloys in austenitic and martensitic states are compared with a pure titanium Ti40 through orthogonal cutting tests. The behavior (cutting forces, apparent friction coefficient) of these materials is observed under different cutting feeds.

2. Method

2.1. Materials

The shape memory alloys are characterized by a solid-state phase change due to temperature or stress variation. This phase change between a β -phase, stable at high temperature, and a martensitic α phase leads to SME and SE. These effects are interesting for biomedical applications, especially TNZ alloys, which are titanium-based SMAs with only non-toxic elements (Ti, Nb, Zr, and Ta) represent an excellent alternative to Ti40, Ti-6Al-4V and NiTi alloys.

The SME occurs when a SMA deformed in martensitic state recovers its initial shape during a heating cycle to reach the austenitic state. The SE occurs when a stress deformation applied in the austenitic state is released. These effects are related to the reversible austenite/martensitic transformation related to temperature and stress (Fig. 1). This transformation is defined by four temperatures:

- As : austenite start
- Af : austenite finish
- Ms : martensite start
- Mf : martensite finish

As and Af are temperatures of start and finish of transition from martensite to austenite state, and Ms and Mf are temperatures of start and finish of transition from austenite to martensite state.

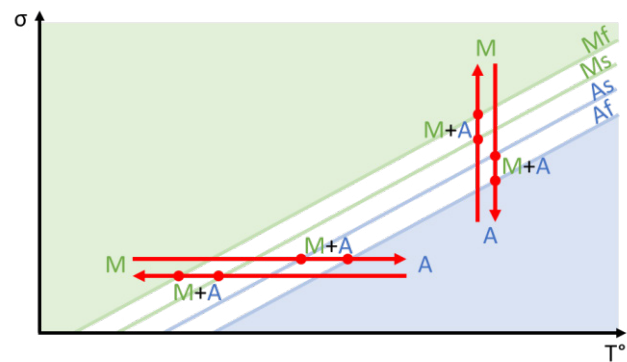


Fig. 1. Reversible martensitic transformation as a function of stress and temperature.

The four temperatures are determined by direct method according to ASTM F2004 [17], by Elmay et al. [18] for Ti24Nb alloy and by Peltier et al. [19] for Ti26Nb. The transformation points are reported in Table 1

Table 1. Transformation temperatures of TiNb alloys.

	ε_{\max} (%)	As (°C)	Af (°C)	Ms (°C)	Mf (°C)
Ti24Nb	32	107	142	97	67
Ti26Nb	20	-17	50	17	30

Ti-24Nb and Ti-26Nb are respectively shape memory alloy and superelastic alloy, with a low Young's modulus (50GPa) that can reach a lower one by controlling the microstructure.

Ti-26Nb and Ti-24Nb SMAs are produced by melting pure titanium and pure niobium. All the alloys studied are prepared in a cold crucible levitation melting furnace under a controlled atmosphere of pure argon. To homogenize the composition, alloys are remelted ten times.

A homogenization heat treatment is performed at 1100°C for 15 hours and then a solution heat treatment is carried out in the same furnace at 850°C for 1 hour. Heat treatment is followed by a water quenching.

Young's modulus of the three materials are given in Table 2. Stiffness of Ti-24Nb and Ti-26Nb are lower than Ti40.

Table 2. Young's modulus of the three materials.

	E (GPa)
Ti24Nb	50
Ti26Nb	45
Ti40	110

2.2. Cutting experiments

The experimental set-up consists of turning a thin tubular sample, shown on fig. 2 to achieve micro-turning assumptions [20]:

- the uncut chip thickness must be small compared to the width of cut (w) to neglect the boundary effects.
- the width should not be too large to consider a constant cutting speed along the cutting edge (variation < 10%).

In this way, an average diameter of 6.366 mm and a thickness w of 318 μm are used. The diameters are directly machined before test on a small height, in order to limit sample run-out and deflection during the test.

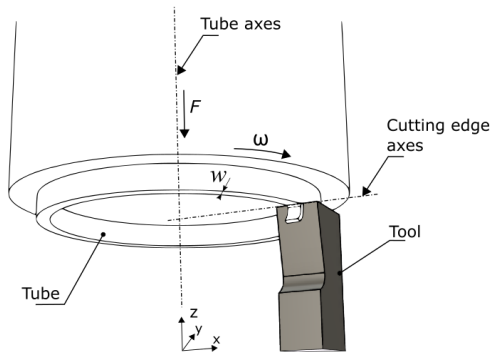


Fig. 2. Micro-cutting set-up

Micro orthogonal cutting tests were performed on a 5 axis CNC vertical milling Rödgers RXP200DS, used as a precision turning lathe and an Ifanger MTNY 41015-R cutting tool for frontal groove (inclination 0°) was used. Rake angle (8°) and cutting-edge radius (r_β 1.5 μm) were measured on Alicona Infinite Focus 3D microscope. Cutting forces were measured through a dynamometric table Kistler Minidyn 9256C2, associated with a Kistler amplifier 9017 and a NI Labview acquisition system.

The cutting speed was set at 60 m/min and feed h varied from 0.333 to 20 $\mu\text{m}/\text{rev}$. Thus, dimensionless ratio h/r_β casts a wide net in order to be in micro and classic turning. Each test was performed at least 2 times showing a repeatability of less than 10% on the plateau area.

3. Results and discussion

Cutting forces of TiNb alloys are clearly different from Ti40. Regardless of h/r_β , Ti40 provides cutting forces classically observed in literature: a plateau is reached after a rise of each force component. For TiNb alloys, peaks are also visible and can be compared with similar behaviour in pure copper [20] or aluminium alloy [21]. Characteristic forces are shown on fig. 3.

Theoretically, a transient period occurs during a rotation of the sample. The undeformed chip thickness transits from 0 to h , defined by the feed per revolution. At the beginning, a chip is not formed immediately, and ploughing occurs until minimum chip thickness is reached. This minimum chip thickness is largely dependent of cutting edge radius and material behaviour.

During the orthogonal cutting tests in the Ti40 sample and for conditions where the ratio h/r_β is higher than 1 the increase in force takes 0.022s, corresponding to one revolution. For lower ratio, the force rise takes between 4 (0.666 $\mu\text{m}/\text{rev}$) and 10 (0.333 $\mu\text{m}/\text{rev}$) revolutions. During these revolutions, it is assumed that the surface is strain-hardened, that an elastic backward movement is amplified until the chip formation occurs.

A similar phenomenon appears for TiNb alloys. For low h/r_β ratio, the force rise takes between 6 (0.666 $\mu\text{m}/\text{rev}$) and 20 (0.333 $\mu\text{m}/\text{rev}$) revolutions meaning that cumulative feed h is greater than 2 times r_β . This transient phase generates a significant cutting force and feed rate. As for Ti40, this phenomenon disappears when ratio h/r_β is greater than 1

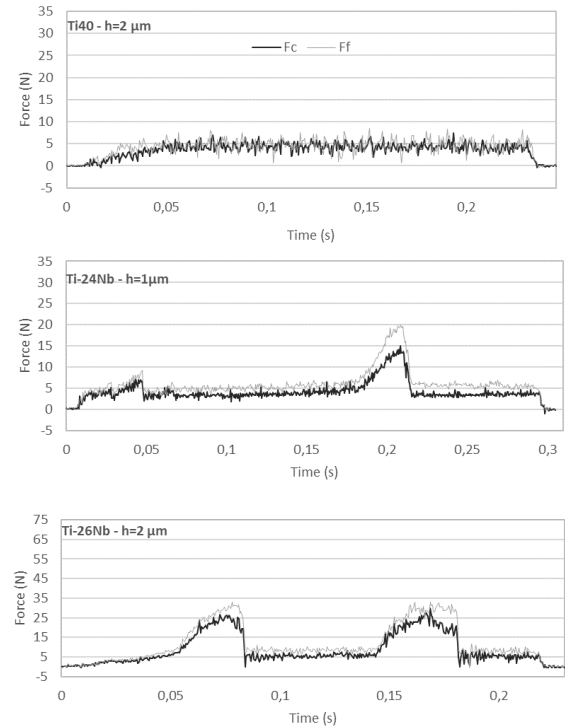


Fig. 3. Characteristic cutting forces for the three materials: Ti40, Ti24Nb and Ti26Nb.

Despite of the peaks on cutting forces, an average value of cutting forces excluding these instabilities can be measured. Fig 4. gives cutting forces as a function of undeformed chip thickness h .

Cutting forces for Ti40 (Fig 4. (a)) are defined by a dominant ploughing zone where feed force is higher than cutting force when h is less than 1 μm , a dominant cutting zone where cutting force is higher than feed force when h is higher than 3 μm and a transient zone with a drop of forces. This behaviour has been already observed in hardened tool steel [22]. This drop is assumed to be the zone where h becomes higher than the hardened layer produced at the previous revolution.

Concerning TiNb alloys, the same behaviour with three zones is observed for Fc. It is not the case for Ff. On the whole range of undeformed chip thickness, feed force is always higher than cutting force, as an indicator of ploughing. The high level of elastic deformation tends to deform material without hardening. Friction between machined surface and clearance face is significant in this case. As a consequence, TiNb alloys are sensitive to burr formation. Burrs are defects that can lead to dust if no deburring is planned.

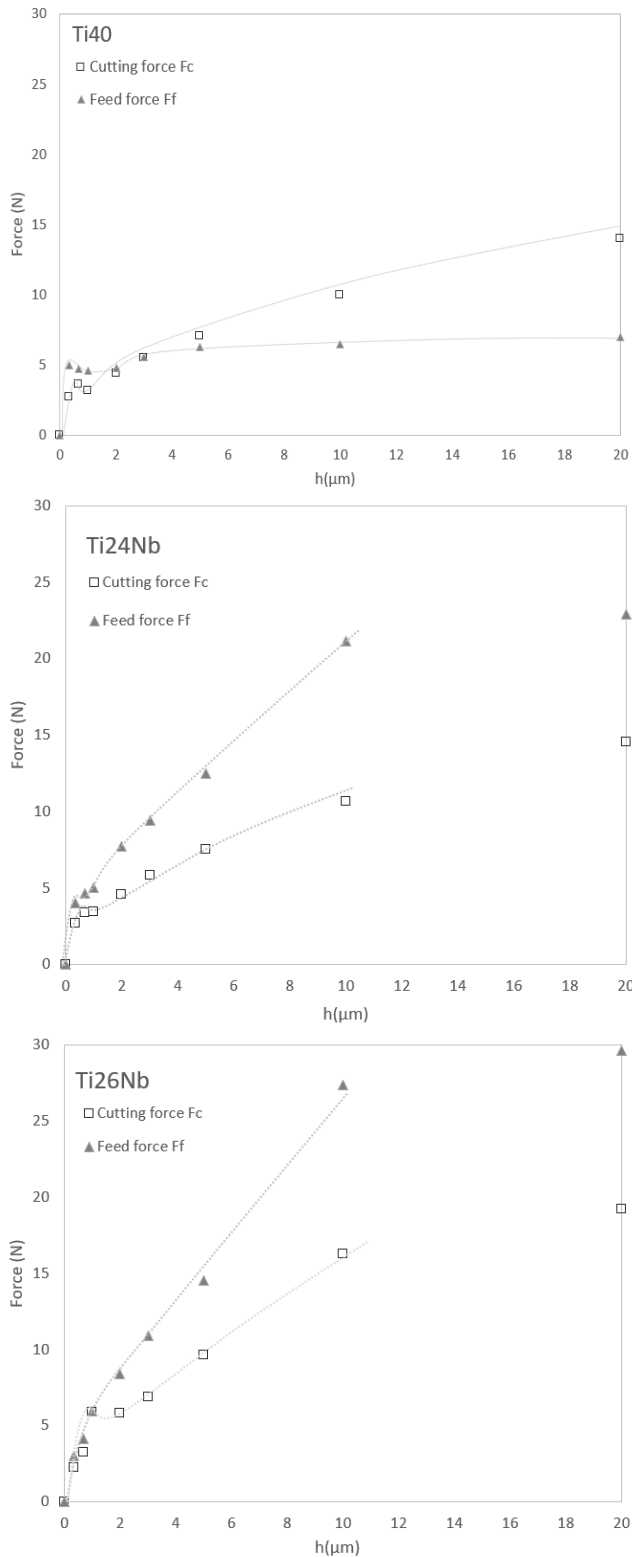


Fig. 4. Cutting forces as a function of h for the three materials: Ti40, Ti24Nb and Ti26Nb.

The peaks observed on cutting forces are related to bulges on chip. An observation of the bulge by SEM is given on Fig. 5. The sliding direction of the rake face on the chip is given by (sd). After a slight thinning of the chip (1), the bulge gets progressively thicker with an increase of shear bands inclination up to 90° (2) and ends with a very rapid thinning (3)

to find a constant chip thickness (4). The bulge is maximum $430\mu\text{m}$ thick, where the chip is less than $100\mu\text{m}$ thick.

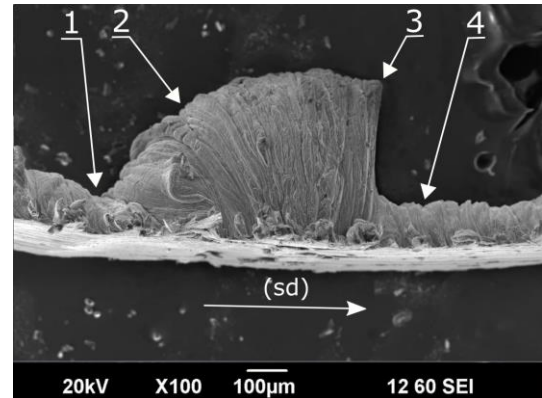


Fig. 5. Bulge observed on a chip

A closed phenomenon was observed when micro-cutting pure copper [23] and aluminum 6061 [21] with a diamond tool, for very small thicknesses h ($<0.8\mu\text{m}$) but for low cutting speeds (1 mm/min) and bigger grains ($50\mu\text{m}$). The authors defined it with the term “scaling”. Scaling occurred after the micro-tool passed through the different regions, at the grain boundary, leading to a smaller shear angle to form a thicker chip. In the case of our experiment, it appears an unstable phase where a large strain may take place in front of the rake face in a very short interval. This involves very severe plastic deformation in front of the rake face. However, it is not the result of a change of crystalline orientation or a passage from one grain to another and even less of a surface phenomenon. Indeed, although in ultra-precision cutting, the phenomenon is observed when cutting a large number of grains over several revolutions of the tubular sample. This bulge formation is attributed to sticking on the rake face, with built-up material. Another clue is the face of the chip in contact with the rake face that show craters whereas the sliding zones are continuous. This phenomenon has to be avoided to limit tool deflection and ensure surface quality.

4. Conclusion

In this study, a comparison of the behaviour during orthogonal cutting tests of Ti40, Ti-24Nb and Ti-26Nb was examined. While Ti40 behaviour is classic, TiNb alloys show particularities.

When entering the material TiNb alloys reach constant forces when h is greater than 2 times $r\phi$. A typical value of 1 is classically observed. This phenomenon is assumed to be related to high ductility and superelasticity of the alloys.

Ploughing is widely present and a risk of burr generation is therefore very high. Moreover, the feed force F_f is systematically higher than the cutting force when cutting TiNb alloys and is an indication of a high elastic recovery.

Cyclic peaks of forces appear during the cutting of TiNb alloys. These peaks are characterized by chip bulges with a progressive increase in its thickness and with a very rapid thinning at its ends, such as a built-up chip sticking at the rake face.

In conclusion, TiNb alloys are difficult to machine, due to their unconventional behaviour. Further investigations will give the best cutting conditions (lubrication, machining assistance...).

References

- [1] N. Sumitomo, K. Noritake, T. Hattori, K. Morikawa, and S. Niwa, Experiment Study on Fracture Fixation with Low Rigidity Titanium Alloy, *J. Mater. Sci. Mater. Med.*, 2008, 19, p 1581–1586
- [2] L. Girod, V. Berry-Kromer, T. Ben Zineb, A. Eberhardt, E. Patoor, and B. Prandi, Evaluation of the immediate post-operative bone-implant condition of a proximal interphalangeal joint prosthesis by a comparative FEA modelling, *Int. J. Interact. Des Manuf.*, 2010, 4, p 157–167
- [3] R. M. Pilliar, H. U. Cameron, A. G. Binnington, J. Szivek, and I. Macnab, “Bone ingrowth and stress shielding with a porous surface coated fracture fixation plate,” *J. Biomed. Mater. Res.*, vol. 13, no. 5, pp. 799–810, 1979.
- [4] M. C. Kennady, M. R. Tucker, G. E. Lester, and M. J. Buckley, “Stress shielding effect of rigid internal fixation plates on mandibular bone grafts. A photon absorption densitometry and quantitative computerized tomographic evaluation,” *Int. J. Oral Maxillofac. Surg.*, vol. 18, no. 5, pp. 307–310, 1989.
- [5] A. Gefen, “Computational simulations of stress shielding and bone resorption around existing and computer-designed orthopaedic screws,” *Med. Biol. Eng. Comput.*, vol. 40, no. September 2001, 2002
- [6] J. Nagels, M. Stokdijk, and P. M. Rozing, “Stress shielding and bone resorption in shoulder arthroplasty,” *J. Shoulder Elb. Surg.*, vol. 12, no. 1, pp. 35–39, 2003.
- [7] P.R. Walker, J. LeBlanc, and M. Sikorska, Effects of Aluminum and Other Cations on the Structure of Brain and Liver Chromatin, *Biochemistry*, 1989, 28, p 3911–3915
- [8] S. Yumoto, H. Ohashi, H. Nagai, S. Kakimi, Y. Ogawa, Y. Iwata, and K. Ishii, Aluminum Neurotoxicity in the Rat Brain, *Int. J. PIXE*, 1992, 2, p 493–504
- [9] S. Rao, T. Ushida, T. Tateishi, Y. Okazaki, and S. Asao, Effect of Ti, Al, and V Ions on the Relative Growth Rate of Fibroblasts (L929) and Osteoblasts (MC3T3-E1) Cells, *Biomed. Mater. Eng.*, 1996, 6, p 79–8
- [10] P. Laheurte, W. Elmay, F. Prima, and T. Gloriant, “Titane et alliages des matériaux de choix pour les applications médicales,” *Tech. l’ingénieur*, vol. 33, no. 0, 2014.
- [11] W. Elmay et al., “Effects of thermomechanical process on the microstructure and mechanical properties of a fully martensitic titanium-based biomedical alloy,” *J. Mech. Behav. Biomed. Mater.*, vol. 18, pp. 47–56, 2013.
- [12] Mitsuo N (2003) Recent research and development in titanium alloys for biomedical applications and healthcare goods. *SCI TECHNOL ADV MAT* 4:445–454
- [13] Ezugwu, E. O., & Wang, Z. M. (1997). Titanium alloys and their machinability—a review. *Journal of materials processing technology*, 68(3), 262–274.
- [14] Weinert, K., Petzoldt, V., 2004. Machining of NiTi based shape memory alloys 378, 180–184. <https://doi.org/10.1016/j.msea.2003.10.344>
- [15] Weinert, K., Petzoldt, V., 2007. Machining NiTi micro-parts by micro-milling 4–7. <https://doi.org/10.1016/j.msea.2006.10.220>
- [16] Piquard, R., Acunto, A.D., Laheurte, P., Dudzinski, D., 2014. Micro-end milling of NiTi biomedical alloys , burr formation and phase transformation. *Precis. Eng.* 38, 356–364. <https://doi.org/10.1016/j.precisioneng.2013.11.006>
- [17] ASTM F 2004 (2008) Standard Test Method for Transformation Temperature of Nickel-Titanium Alloys by Thermal Analysis
- [18] Elmay, W. (2013). Développement de nouveaux alliages biocompatibles instables mécaniquement à bas module d'Young (Doctoral dissertation, Ecole nationale supérieure d'arts et métiers-ENSAM).
- [19] Peltier L, Berveiller S, Meraghni F, et al (2021) Martensite Transformation and Superelasticity at High Temperature of (TiHfZr)74(NbTa)26 High-Entropy Shape Memory Alloy. *Shape Mem Superelasticity* 74:. <https://doi.org/10.1007/s40830-021-00323-4>
- [20] Piquard, R. (2016). Expérimentation et modélisation de la micro-coupe pour une application au micro-fraisage (Doctoral dissertation, Besançon).
- [21] Ding, X., & Rahman, M. (2012). A study of the performance of cutting polycrystalline Al 6061 T6 with single crystalline diamond micro-tools. *Precision Engineering*, 36(4), 593–603.
- [22] Piquard, R., Thibaud, S., D’Acunto, A., Fontaine, M., & Dudzinski, D. (2017). Phenomenological modelling of micro-cutting based on experimental results. *The International Journal of Advanced Manufacturing Technology*, 88(9), 3429–3436.
- [23] Ding, X., Jarfors, A.E.W., Lim, G.C., Shaw, K.C., Liu, Y.C., Tang, L.J (2012). A study of the cutting performance of poly-crystalline oxygen free copper with single crystalline diamond micro-tools. *Precis. Eng.* 36, 141–152.